Disruptions in the High-β Spherical Torus NSTX

S.P. Gerhardt[1], M. G. Bell[1], R.E. Bell[1], A.H. Boozer[2], E. Fredrickson[1], E. Kolemen[1], B. P. Le Blanc[1], R. Maingi[2], J. Manickam[1], A. McLean[4], J.E. Menard[1], D. Mueller[1], R. Raman[5], S. A. Sabbagh[3], V. Soukhanovskii[4], H. Yuh[6]

[1]Princeton Plasma Physics Laboratory, Princeton NJ, 08540 USA
[2]Columbia University, New York NY, 10027 USA
[3]Oak Ridge National Laboratory, Oak Ridge TN, 37831 USA.
[4]Lawrence Livermore National Laboratory, Livermore CA, 94550 USA
[5]University of Washington, Seattle, WA, 98195 USA
[6]Nova Photonics, Princeton NJ, 08540 USA

E-mail contact of main author: sgerhard@pppl.gov

Abstract. Result on disruptivity statistics, disruption predictability, and halo current physics from the National Spherical Torus (NSTX) are presented. We find that the minimum disruptivity occurs at high-β_N, with strong shaping, broad current and pressure profiles, and with rotation maintained above a threshold level. Elevation of q_{min} (>~1.2) and avoidance of transients is critical for the avoidance of core n=1 kink/tearing modes. Many disruptions can be predicted based on observations of quantities like the n=1 poloidal field perturbation, neutron emission, loop voltage, and vertical motion. When these measurements are combined into a simple predictor, the sum of missed disruptions and false positives can be reduced to a value of ~6%. Halo currents in NSTX are observed to be strongly asymmetric, with periods of strong toroidal rotation. Rotation frequencies up to 2 kHz, and cases with up to 8 toroidal transits of the asymmetry, have been observed. The rotation frequency and number of rotations tends to be smallest when the halo currents are large.

1. Introduction

Disruptions [1], the rapid loss of thermal energy followed by a quench of the plasma current, are unfortunately common occurrences in tokamaks and spherical torus devices. They are ultimately due to the crossing of some MHD stability boundary, though the first event in the sequence leading to a disruption may or may not be related to MHD. In addition to the loss of discharge time, impacting present scientific productivity and future power production, disruptions can damage the tokamak by the generation of eddy currents [2], impulsive thermal loading [1,2], runaway electron beam generation & deconfinement [1], or halo current loading [1,2].

This paper addresses three aspects of disruptions, using data from the high-β spherical torus NSTX. Section 2 presents an analysis of the disruptivity of NSTX discharges [3]. Section 3 addresses the detectability of disruptions in NSTX. Section 4 describes measurements of disruption halo currents in NSTX [4,5].

2. Disruptivity Analysis of NSTX Plasmas

There are two common measures of the tendency of the plasma to disrupt [6]. The first is the disruption rate, defined as the fraction of all discharges that experience a disruption at any point in the discharge. The second is the disruptivity, defined as the number of disruptions when the plasma is in a given portion of parameters space, divided by the total amount of time that the plasma is in that part of parameter space. A database of NSTX disruption rate and disruptivity statistics has been developed, using discharges from the 2006 through 2010 campaigns [3]. The disruptivity is based on sampling the NSTX data every 33.3 ms. The

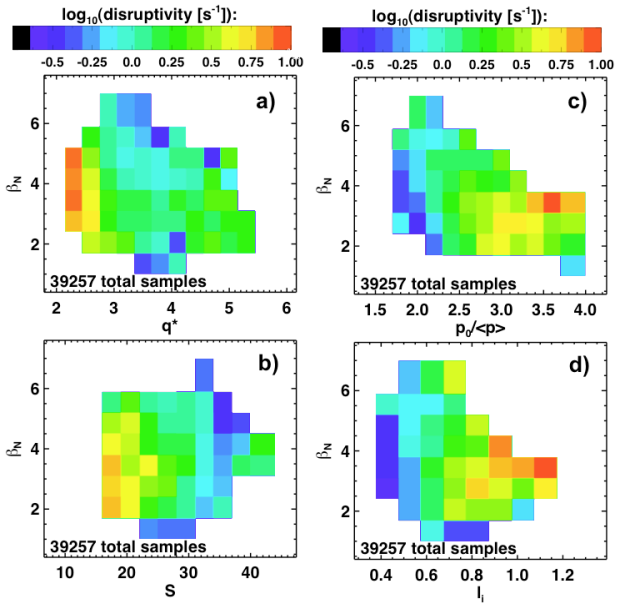

Fig. 1) Disruptivity as a function of β_N and a) q, b) shape factor, c) pressure peaking factor, and d) internal inductance.*

disruptivity and associate disruption causes will be discussed in this paper. Note that the time of the disruption in this section is defined in terms of the first substantial negative deviation of the plasma current; this time is often somewhat earlier than the final current quench, but has the advantage of being more representative of the plasma conditions that prompt the disruption.

Fig. 1 shows the disruptivity in NSTX as a function of β_N and a single additional parameter. In frame a), the additional parameters is $q^* = \varepsilon\pi a B_T\left(1+\kappa^2\right)/\mu_0 I_P$, where ε is the inverse aspect ratio, a is the minor radius, κ is the boundary elongation, B_T is the toroidal field, and I_P is the plasma current. We see a rapid increase in disruptivity for q^*<2.4, but no increase in disruptivity at higher β_N. Note that this q^* value is surprisingly higher than the ideal MHD boundary of ~1.7 [7]. The reason for this increase in disruptivity is a wide range of operational problems at the highest current or with low shaping [3]. It should be noted that attempts to access this very low q* regime have been limited in the campaigns under consideration here, although they were more common in the initial years of NSTX operations [8]. Frame b) shows the disruptivity vs. β_N and shape parameter $S = q_{95} I_P / a B_T \propto \varepsilon\left(1+\kappa^2\right) f\left(\kappa,\delta,\varepsilon,...\right)$ [9]; boundary shapes with low aspect ratio, high elongation, and high triangularity, all of which are typically beneficial for stability, will have large values of S. The figure does indeed show a great reduction of disruptivity with shaping. Finally, Fig. 1c) and 1d) show the disruptivity vs. two parameters related to the peaking of the profiles: the pressure peaking, defined as the central pressure normalized to the volume averaged pressure $F_P = p_0/\langle p\rangle$, and the internal inductance $l_i(1) = l_p^2 \iiint B_P^2 dV \Big/ V\left(\mu_0 I_P\right)^2$, where l_P is the poloidal circumference of the boundary and V is the volume. These quantities are larger when the pressure and current profiles are more peaked. We see clearly that operating at large pressure peaking, especially at higher values of β_N, results in a strong increase in disruptivity. Note that increases in the pressure peaking are well known to result in a reduction of the ideal stability limit [10-13]. Similarly, while higher l_i generally increases the no-wall limit for broad pressure profiles [10], NSTX often operates in the wall-stabilized regime [7,11,12,14,15], where broad current profiles improve the coupling to passive conductors.

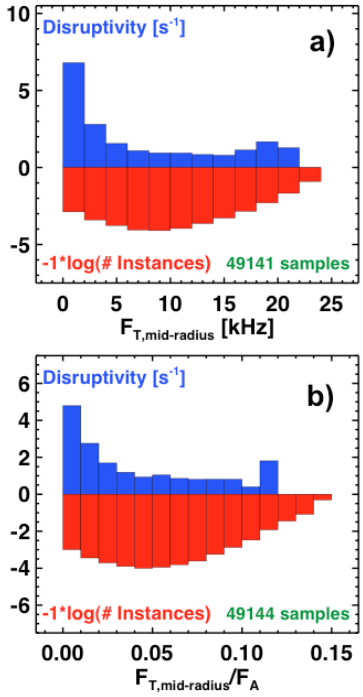

Fig. 2) Disruptivity as a function of the a) actual and b) normalized toroidal rotation.

Beyond strong shaping and broad profiles, maintenance of the plasma rotation is required in order to avoid disruptions. This is shown in Fig. 2, where the

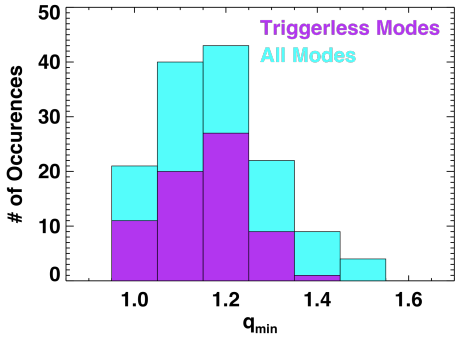

Fig. 3) Histogram of q_{min} at the onset of core n/m=1/1+2/1 modes.

disruptivity is shown as a function of rotation at the approximate radius of the q=2 surface. In frame a), it is clear that rotation frequencies below ~ 5kHz lead to an increased disruption rate. Frame b) shows the same data, but where the frequency is normalized to the Alfven frequency $F_A = V_A / 2\pi R_0$ (with $V_A = |B_0| / \sqrt{2\mu_0 \bar{n}_e m_P}$), as this normalization is commonly used in resistive wall mode (RWM) studies [15]. We find that the disruptivity is substantially increased for $F_{T,mid-radius} / F_A < 0.03$. Some increase in the disruptivity at low rotation is due to the onset of RWMs at high β_N. A second reason is the onset and locking of core n=1 modes.

NSTX high-β, H-mode plasmas essentially never exhibit sawteeth. Rather, as q_{min} approaches unity, they develop core n=1 kink modes [16], often coupled to 2/1 magnetic islands [13] that display characteristics of a neoclassical tearing mode (NTM) [17]. These modes can be triggered by energetic particle modes (EPMs) or ELMs, or can onset without any clear triggering perturbation. From the perspective of this paper, the question is how much must q_{min} be above unity to avoid the onset of these modes.

The answer to this is provided in Fig. 3, where a histogram of q_{min} at mode onset is plotted, for a database of 138 high-power H-mode discharges, based on MSE-constrained equilibrium reconstructions. Those cases without clear triggering perturbations typically show mode onset with $1.0<q_{min}<1.2$. However, those cases with triggers can have mode-onset at substantially higher values of q_{min}, up to 1.4. This underscores the importance of maintaining both elevated q_{min} and avoidance of core and edge transients in order to maintain high-performance.

3. Detectability of Disruptions in NSTX

Having established the regimes where disruptions are more or less likely to occur, it is useful to consider whether these disruptions can be detected in advance. We do this by first examining how well single parameters can predict a disruption, and then how simple combinations of these single parameter tests can improve the predictive capability. In this section, the disruption is defined by the start of the current quench [17], and only causal interpolation and filters are used. This work will be expanded to a larger paper in the future.

With regard to single parameters, we have examined the time to disruption after a given

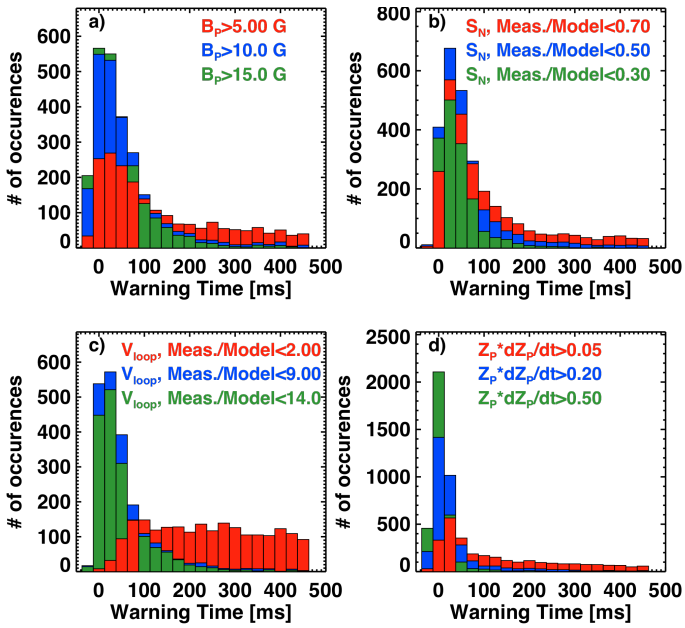

Fig. 4) Histograms of time between thresholds being crossed and the current quench. Tests are based on a) n=1 poloidal field sensors, b) the neutron rate, c) the loop voltage, and d) the vertical motion.

criterion is met; for instance, "time to disruption after the external n=1 mode sensor exceeds 10 Gauss", or "time to disruption after the rotation drops beneath 5 kHz". Different diagnostic signals have been examined using different threshold levels, allowing a study of which signals are indicative of approach to disruption.

Fig. 4a shows the results of such a test using the n=1 poloidal field RWM sensors [15]; these are conceptually similar to the "locked" mode sensors often used to trigger mitigation systems [6]. We find that threshold levels of 5 Gauss produce an unacceptable number of false positives, defined here as a warning more that 300 ms before the disruption. Increasing the threshold to 8 and then 14 G dramatically reduces the false positive count, but also increases the number of missed disruptions, defined here as the threshold being reached later than 10 ms before the current quench. While these sensors are good predictors of disruption, further data is required in order to improve the prediction.

Where possible, we have tried to use some physics-based modeling to develop additional threshold tests. Fig. 4b) shows a case where the measured neutron emission is compared to the prediction from a rapidly evaluated slowing-down model; the injected beam power and voltage, density and temperature from Thomson scattering, and Z_{eff} from visible bremsstrahlung are used in the evaluation of the model. Ratios of measurement to model of 0.7 predict many false positives, due to features like fast-particle MHD leading the reductions in the neutron rate [19], or errors in the Z_{eff} measurement. When the threshold ratio is reduced to 0.5 or 0.3, this measure becomes a reasonably useful indicator of proximity to disruption, as it is indicative of near complete loss of the fast particle population.

The current drive power required to maintain the target plasma current is another potential measure of the plasma health. The plasma current in NSTX is maintained by adjusting the loop voltage via a PID feedback loop. The neutral beam heating, which controls the neutral beam current drive and, with the transport level, the bootstrap current, was pre-programmed in the majority of NSTX discharges [13,20]. We used the measured neutral beam parameters, plasma current and toroidal field, electron density, and boundary geometry to estimate an average electron temperature assuming confinement follows the ITER-$98_{y,2}$ scaling expression [21]. The neutral beam and bootstrap currents are then estimated using 0D expressions previously calibrated against detailed TRANSP calculations. The ohmic current is then estimated as the total current minus the non-inductive sources, with the predicted loop voltage following once the resistivity is estimated.

Fig. 4c) shows results using the ratio of measured to modeled loop voltage as indicator of proximity to disruption. Factor of 2 fluctuations in the loop voltage are commonly produced by the feedback system; using a causal filter to remove those fluctuations introduces undesirable delays. On the other hand, using large threshold values results in a reasonable predictor for the disruption. Fundamentally, the reason is that the typical large pre-disruption thermal energy losses [1,3] result in a significantly higher loop voltage than would be expected during the high confinement phase.

Finally, Fig. 4d) shows a parameter related to vertical stability: this is the product of Z_P and dZ_P/dt, which has the desirable property of being large when the plasma is above the midplane and moving upwards, or below the midplane and moving downward. Here, both Z_P and dZ_P/dt are estimated from the flux and voltage on two poloidal flux loops on the outboard side of the plasma, one above the midplane and one beneath. It is clear that values of $Z_P \cdot dZ_P/dt$ greater than ~0.2 are indicative of the loss of vertical stability.

The frames if Fig. 4 show an additional point; setting thresholds that reduce the false positive count results in an increase in the missed disruption rate. On the other hand, threshold values with a large false positive count will generally be best at avoiding missed disruptions.

While the above tests have connection to physics quantities and are easily implemented in realtime, they are only a first step in developing "physics based" realtime

tokamak disruption monitoring. For instance, more sophisticated realtime estimates of the fast particle populations and current drive sources should be implemented for comparison to measurements; an initial step in this direction can be seen in Ref. [22]. Realtime estimates of the vertical stability margin should be calculated, to complement plasma position measurements. Realtime measures of n=1 stability via resonant field amplification [23] may be a possibility for assessing proximity to the disruptive stability limit.

These results illustrate that no single diagnostic can predict disruption onset with the reliability required for future tokamak operations; a combination of the signals is required. The most common approach to solving this problem has been to use a neural network (see Ref. [1] and references therein). Here, we examine a different approach.

For each of 17 threshold tests of the style described above, the levels that give 10%, 5%, 2%, 1% and 0.5% false positive rates have been identified. There is a certain value of "points" associated with each of these thresholds; in the present case, point values from 1 up to 5 are associated with thresholds providing false positive rates of 10% down to 0.5%. At each 2 ms time step, the 17 different threshold tests are evaluated, and a point value determined for each. These point values are then summed, producing an aggregate point total. Note that this point total will be large if many of the tested quantities have achieved a "dangerous" but not yet disruptive values, or if only a few tests achieved quantities typical of disruption values. When the aggregate total achieves some threshold value, a disruption alarm is declared. Note that the single test point values noted above (1 to 5) have not been thoroughly optimized

An example of these calculations is shown Fig. 5, based on a database of ~1700 disruptions during the I_P flat-top of NBI heated plasmas. By requiring a total of eight points to declare a disruption, the total of missed disruptions and false positives can be reduced to ~6%. It is interesting to consider the sources of these failures, as it is likely that they would provide a problem for any detection scheme. The false positive count is dominated by cases where early rotating MHD modes, developing as the q=4, 3, & 2 surfaces enter the plasma, slow and sometimes lock to the wall [3]. While these events are often disruptive, the discharge sometimes survives after a large β collapse; it is difficult to consider these as true false positives. The missed warning count is largely from locked modes and RWMs.

4. Halo Current Dynamics in NSTX

Disruptions in NSTX typically have some phase of vertical instability. As a result, halo currents [1] are often observed during the late phase of the vertical motion, during and sometimes slightly preceding the current quench. Ref. [18] describes many features of the halo current in NSTX; this section will focus on the dynamics of the halo current asymmetry where the currents enter the divertor [5].

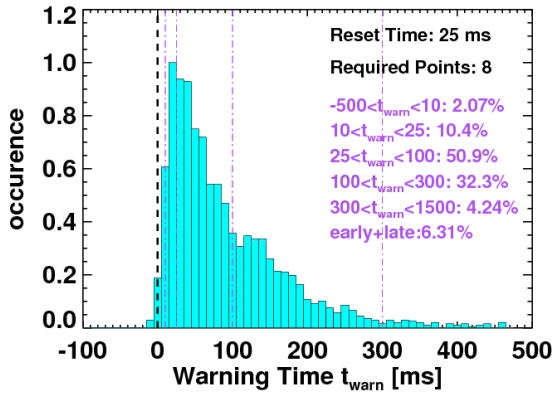

Fig. 5) Histogram of warning times based on the combination of tests.

Many of the important dynamics can be seen in Fig. 6. Frames a) and b) show the plasma current and boundary evolution in the phase leading up to the disruption; this is clearly a downward-going VDE that limits on the outer divertor plate. Frame 6c) shows contours of halo current at the fixed poloidal location, as a function of toroidal angle and time. This current is measured by an array of six "shunt tiles" [4,24], which are located in the red tiles of Fig. 6b), at approximately the center

(radially) of the outboard divertor plate. In this example, the halo currents are first observed to flow at nearly fixed toroidal angle. However, at t~0.411 s, the halo current asymmetry begins to rapidly rotate, completing in this case 4 complete toroidal rotations.

Fig 6c) shows different measures of the halo current magnitude. First, the n=0 and n=1 components are shown, as determined by fits of the equation $J(\phi) = J_{HC,n=0} + J_{HC,n=1}\cos(\phi - \phi_{HC})$ to the data from the six shunt tiles at each time point; here $J_{HC,n=0}$, $J_{HC,n=1}$, and ϕ_{HC} are fit parameters (the parameter ϕ_{HC} is plotted as black, green, and magenta in Fig. 6c) in order to emphasize the phase rotation). The n=0 and n=1 components of the halo current have comparable magnitude through the majority of the pulse; only at the end of the pulse does the asymmetry disappear and an axisymmetric halo current pattern exist. The maximum current measured on any single sensor is also shown in frame c), and is comparable to the sum of the n=1 and n=0 currents. Hence, the dominant structure of the halo current is a single, toroidally localized lobe. Further analysis indicates that typical full width at half maxima for the lobes are 2-4 radians, and that the rotation frequency and spatial width can vary rapidly during the disruption phase [5]. The smooth toriodal rotation in Fig. 6, however, is not always present. Fig. 7 shows the halo current contours for a similar downward VDE, which has multiple starts and stops of the asymmetry rotation.

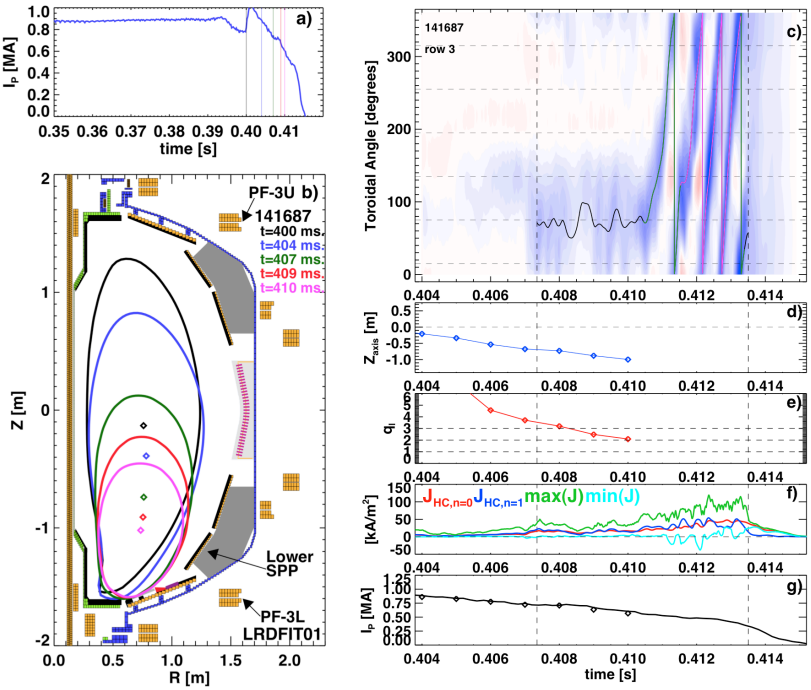

Fig. 6) Example dynamics of the halo current toroidal asymmetry.

Some statistics regarding the observed halo current rotation are shown in Fig. 8. Rotation parameters are shown as a function of two measures of the halo current magnitude; the n=0 amplitude (left), and the maximum local current from any sensor (right). In each case, these current magnitudes are averaged over the period when the n=1 halo current magnitude is greater than 50% of its maximum value. The colors correspond to averaging windows where the n=1 magnitude is greater then 25% (black), 50% (green) and 75% (magenta) of its maximum; these correspond

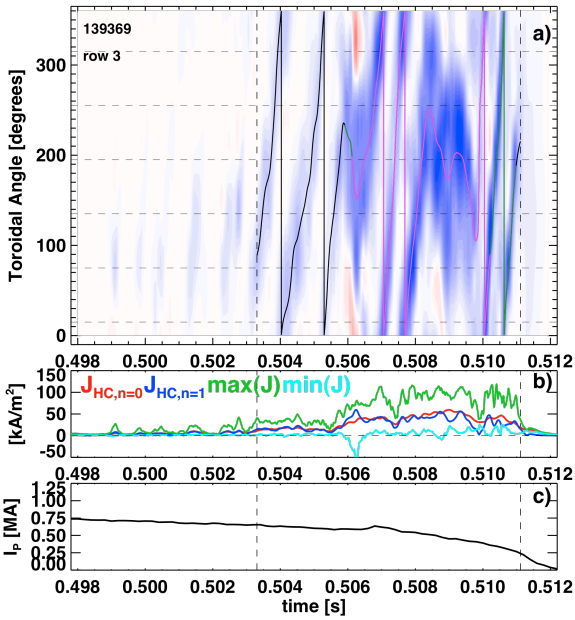

Fig. 7) Example with seemingly erratic halo current asymmetry dynamics

to, in the first case, an average over the majority of the halo current pulse, and in the last case, an average over the period of largest halo currents.

The results in Fig. 8a) and 8b) show that the rotation frequency tends to decrease as the halo current magnitude increases. The typical rotation frequencies using the averaging scheme described above range from no net rotation to values as high as 2 kHz. The typical pulse durations are shown in frames c) and d). The pulses tend to be shorter for higher amplitude halo currents. These results are combined in frames e) and f), which show that the typical number of revolutions decreases as the halo current magnitudes are increased. Cases with up to 8 rotations have been observed with rather low levels of halo current. However, for the highest level of halo current, less than 2 revolutions have been observed.

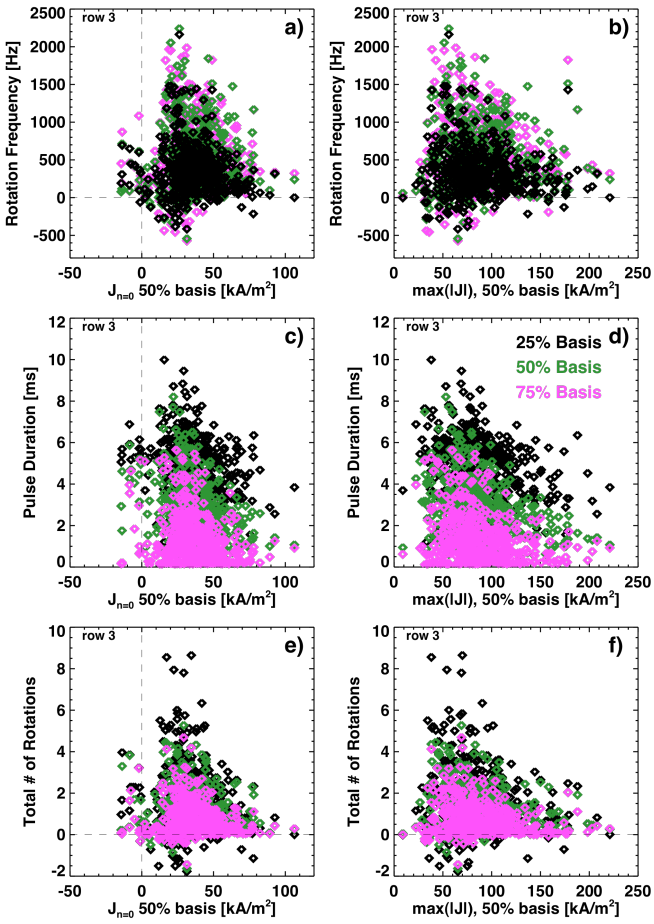

Fig. 8) Scatter plots of the halo current rotation frequency in a) & b), pulse duration in c) and d), and total # of revolutions in e) and f).

Figs. 6 & 8 also show a trend for the halo current to become toroidally symmetric at the end of the disruptions. In order to understand this phase, we have used an axisymmetric filament model to predict the poloidal flux contours during this late phase of the disruption. This model makes no assumptions about the plasma current magnitude outside the last closed magnetic surface (unlike a typical Grad-Shafranov solver, which assumes that there is no current in that region), includes vessel toroidal currents as quantities to be fit, and uses a regularization procedure to prevent unphysical spatial variations in the currents. These results indicate that the phase with nearly axisymmetric halo currents starts when the vertically drifting magnetic axis has nearly or completely vanished, and open field line currents dominate the system.

This research was funded by the United States Department of Energy under contract DE-AC02-09CH11466.

References

[1] HENDER, T.C., et al., "Chapter 3: MHD stability, operations limits and disruptions", Nucl. Fusion **47** (2007) S128.

[2] SUGIHARA, M., et al., "Disruption Scenarios, their mitigation and operation windows in ITER", Nucl. Fusion **47**, (2007) 337.

[3] GERHARDT, S.P., et al, "Disruptions, Disruptivity, and Safer Operating Windows in the High-β Spherical Torus NSTX", submitted to Nuclear Fusion (2012).

[4] GERHARDT, S.P., et al. "Characterization of Disruption Halo Currents in the National Spherical Torus Experiment", Nuclear Fusion **52**, (2012) 062005.

[5] GERHARDT, S.P., et al, "Dynamics of the disruption halo current toroidal asymmetry in NSTX", submitted to Nuclear Fusion (2012).

[6] DEVRIES, P.C., et al., "Statistical analysis of disruptions in JET", Nucl. Fusion **49**, (2009) 055011.

[7] MENARD, J.E., et al., "Aspect ratio scaling of ideal no-wall stability limits in high bootstrap fraction tokamak plasmas", Phys Plasmas **11** (2004) 639.

[8] GATES, D.A., "High β, long pulse, bootstrap sustained scenarios on the National Spherical Torus Experiment (NSTX)", Phys. Plasmas **10** (2003) 1659.

[9] LAZARUS, E. A., et al., "An optimization of beta in the DIII-D tokamak", Phys. Fluids B **4** (1992) 3644.

[10] HOWL, W, et al., "Sensitivity of the kink instability to the pressure profile" Phys Plasmas B **4** (1992) 1724.

[11] SABBAGH, S.A., "Beta-limiting instabilities and global mode stabilization in the National Spherical Torus Experiment" Phys. Plasmas **9** (2002) 2085.

[12] SABBAGH, S.A., "The resistive wall mode and feedback control physics design in NSTX" Nucl. Fusion **44** (2004) 560.

[13] GERHARDT, S.P., et al, "Recent progress towards an advanced spherical torus operating point in NSTX", Nuclear Fusion **51**, (2011) 073031.

[15] SONTAG, A.C., et al., "Resistive wall mode stabilization of high-b plasmas in the National Spherical Torus Experiment", Phys. Plasmas **12** (2005) 056112.

[16] MENARD, J.E., et al., "Internal kink mode dynamics in high-β NSTX plasmas" Nuclear Fusion **45** (2005) 539.

[17] GERHARDT, S.P., et al., "Relationship between onset thresholds, trigger types, and rotation shear for the m/n=2/1 neoclassical tearing mode in a high-βA spherical torus", Nuclear Fusion **49** (2009) 032003.

[18] GERHARDT, S.P., et al., "Characterization of the plasma current quench during disruptions in the National Spherical Torus Experiment", Nucl. Fusion **49** (2009) 032003

[19] FREDRICKSON, E.D., "Collective fast ion instability-induced losses in the National Spherical Tokamak Experiment", Phys. Plasmas **13** (2006) 056109.

[20] GERHARDT, S.P. et al., "Implementation of β_N control in the National Spherical Torus Experiment", Fusion Science & Tech. **61** (2012) 11

[21] ITER Physics Expert Groups on Confinement and Transport and Confinement Modelling and Database, et al., "Chapter 2: Plasma confinement and transport", Nuclear Fusion **39** (1999) 2175.

[22] FELICI, F., et al., "Real-time physics-model-based simulations of the current density profile in tokamak plasmas", Nuclear Fusion **51** (2011) 083052.

[23] REIMERDES, H., et al., "Measurement of resistive wall mode stability in rotating high-β DIII-D plasmas", Nuclear Fusion **45** (2005) 368.

[24] GERHARDT, S.P., et al., "Techniques for the measurement of disruption halo currents in the National Spherical Torus Experiment", Rev. Sci. In strum **82**, (2011) 103502.